

ULRR

Reversible switching between highly porous and non-porous phases of an interpenetrated diamondoid coordination network that exhibits gate-opening at methane storage pressures

Item Type	Article
Authors	Yang, Qing#Yuan;Lama, Prem;Sen, Susan;Lusi, Matteo;Chen, Kai-Jie;Gao, Wen-Yang;Shivanna, Mohana;Pham, Tony;Hosono, Nobuhiko;Kusaka, Shinpei;Perry, John J.;Ma, Shengqian;Space, Brian;Barbour, Leonard J.;Kitagawa, Susumu;Zaworotko, Michael J.
Citation	Angewandte Chemie;54, pp. 7042-7045
Publisher	John Wiley & Sons, Inc.
Download date	2026-04-22 23:28:13
Item License	https://creativecommons.org/licenses/by-nc-sa/1.0/
Link to Item	https://hdl.handle.net/10344/6940

Accepted Article

Title: Reversible switching between highly porous and non-porous phases of an interpenetrated diamondoid coordination network that exhibits gate-opening at methane storage pressures

Authors: Michael Zaworotko, Qingyuan Yang, Prem Lama, Susan Sen, Matteo Lusi, Kai Jie Chen, Wenyang Gao, Mohana Shivanna, Tony Pham, Shinpei Kusaka, Nobuhiko Hosono, John Perry, Shengqian Ma, Brian Space, Leonard Barbour, and Susumu Kitagawa

This manuscript has been accepted after peer review and appears as an Accepted Article online prior to editing, proofing, and formal publication of the final Version of Record (VoR). This work is currently citable by using the Digital Object Identifier (DOI) given below. The VoR will be published online in Early View as soon as possible and may be different to this Accepted Article as a result of editing. Readers should obtain the VoR from the journal website shown below when it is published to ensure accuracy of information. The authors are responsible for the content of this Accepted Article.

To be cited as: *Angew. Chem. Int. Ed.* 10.1002/anie.201800820
Angew. Chem. 10.1002/ange.201800820

Link to VoR: <http://dx.doi.org/10.1002/anie.201800820>
<http://dx.doi.org/10.1002/ange.201800820>

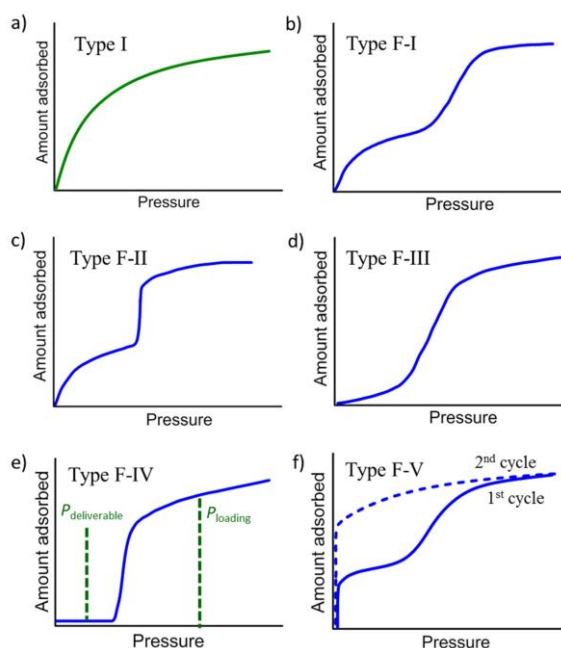
Reversible switching between highly porous and non-porous phases of an interpenetrated diamondoid coordination network that exhibits gate-opening at methane storage pressures

Qing-Yuan Yang,^[a] Prem Lama,^[b] Susan Sen,^[c] Matteo Lusi,^[a] Kai-Jie Chen,^[a] Wen-Yang Gao,^[d] Mohana Shivanna,^[a] Tony Pham,^[d] Nobuhiko Hosono,^[c] Shinpei Kusaka,^[c] John J. Perry IV,^[a] Shengqian Ma,^[d] Brian Space,^[d] Leonard J. Barbour,^[b] Susumu Kitagawa,^[c] and Michael J. Zaworotko^{*[a]}

Abstract: Some porous materials can reversibly change their crystal structure in response to interfacial sorbate/sorbent interactions. Here, we report that a new flexible coordination network, **NiL₂** (L = 4-(4-Pyridyl)-biphenyl-4-carboxylic acid), with diamondoid, **dia**, topology switches between non-porous (closed) and several porous (open) phases at specific carbon dioxide (CO₂) and methane (CH₄) pressures. These phases are manifested by multi-step low pressure isotherms for CO₂ or a single-stepped high pressure isotherm for CH₄. The potential methane working capacity of **NiL₂** approaches that of compressed natural gas but at much lower pressures. The guest induced phase transitions of **NiL₂** were studied by single-crystal X-ray diffraction (SC-XRD), *in-situ* variable pressure powder XRD (PXRD), synchrotron powder XRD (SXRD), pressure-gradient differential scanning calorimetry (P-DSC) and molecular modeling. The collection of detailed structural information facilitates insight into the extreme flexibility of **NiL₂**. Specifically, the extended linker ligand, “X-ligand”, L, undergoes ligand contortion and interactions between interpenetrated networks or sorbate-sorbent interactions enable the observed switching between closed and open phases, respectively. We consider **NiL₂** to be prototypical for a large family of related porous materials.

Crystalline solids are generally regarded as being rigid. However, porous materials such as zeolites^[1] and porous coordination networks^[2a] can exhibit guest induced structural transformations when exposed to appropriate stimuli. The degree of flexibility exhibited by such materials can be extreme in porous coordination networks, which are also known as porous coordination polymers (PCPs),^[2] metal-organic materials (MOMs)^[3] or metal-organic frameworks (MOFs).^[4] Flexible microporous materials^[5-9] challenge classical sorption classifications because they necessarily change their pore geometry as a consequence of a structural change. For example,

whereas type-I (Langmuir) adsorption isotherms (Scheme 1a) are characteristic of rigid microporous materials, flexible microporous materials tend to exhibit ‘stepped’ or ‘S-shaped’ isotherm profiles caused by breathing^[6a] or swelling.^[6b] When porous after activation the pressure at which the step occurs coincides with a structural transformation between less open and more open phases via gradual opening (Scheme 1b, type F-I)^[6a] or sudden opening (Scheme 1c, type F-II).^[6c] Transformation from a non-porous (closed) activated phase to a porous (open) phase can also occur gradually (Scheme 1d, type F-III) or suddenly (Scheme 1e, type F-IV).^[7] Type F-IV isotherms are desirable for pressure swing gas storage, including adsorbed natural gas (ANG) storage.^[7d] This is because type I, F-I, F-II and F-III isotherms (Scheme 1a-1d) retain adsorbed gas at low pressures, thereby reducing working capacity. Unfortunately, whereas there are now ca. 100 flexible metal-organic materials,^[5b] FMOMS, only 2 FMOMS^[7c, 7d] exhibit F-IV isotherms and high uptake (>250 cc/cc). Kaskel’s group reported [Ni₂(2,6-ndc)₂(dabco)], DUT-8(Ni),^[7c] and Co(bdp) (bdp²⁻=1,4-



Scheme 1. Proposed classification of isotherm profiles for flexible microporous materials: Type I = rigid microporous material; Type F-I = flexible microporous material (gradual opening from small pore to large pore); Type F-II = flexible microporous material (sudden opening from small pore to larger pore); Type F-III = flexible microporous material (gradual opening from non-porous to porous); Type F-IV = Flexible microporous material (sudden opening from non-porous to porous). Type F-V depicts a shape memory effect^[8c, 9d] and is not relevant herein.

- [a] Dr. Q. Y. Yang, Dr. M. Lusi, Dr. K. J. Chen, Mr. M. Shivanna, Dr. J. J. Perry IV, Prof. Dr. M. J. Zaworotko
Department of Chemical Sciences, Bernal Institute,
University of Limerick
Limerick, Republic of Ireland.
E-mail: Michael.Zaworotko@ul.ie
- [b] Dr. P. Lama, Prof. Dr. L. J. Barbour
Department of Chemistry and Polymer Science, University of
Stellenbosch, Matieland 7602 (South Africa)
- [c] Dr. S. Sen, Dr. N. Hosono, Dr. S. Kusaka, Prof. Dr. S. Kitagawa
Institute for Integrated Cell-Material Sciences (WPI-iCeMS), Kyoto
University, Katsura, Nishikyo-ku, Kyoto 615-8530, Japan
- [d] Dr. W. Y. Gao, Dr. T. Pham, Prof. Dr. S. Ma, Prof. Dr. B. Space
Department of Chemistry, University of South Florida, 4202 East
Fowler Avenue, Tampa, Florida, USA

benzenedipyrazolate) was reported by Long's group.^[7d] The latter is of special interest because it undergoes a structural phase transformation in response to CH₄ pressures between 5–35 atm.^[7d] Herein we introduce a new porous material that exhibits a type F-IV isotherm and high uptake, **NiL₂** (**L** = 4-(4-Pyridyl)-biphenyl-4-carboxylic acid).

Solvothermal reaction of 4-(4-Pyridyl)-biphenyl-4-carboxylic acid (**HL**) (Figure 1a) with Ni(NO₃)₂·6H₂O in DMF at 105 °C afforded crystals of the expected^[10] diamondoid (**dia**) network **NiL₂**, **X-dia-1-Ni**. **L** was prepared through serial Suzuki-Miyaura coupling reactions (Figure S1). Single crystals of as-synthesized **X-dia-1-Ni**, **X-dia-1-Ni-a1**, characterized by SC-XRD revealed that it crystallizes in tetragonal space group *I*₄*cd* with *a* = *b* = 24.2018(6) Å, *c* = 16.2670(8) Å, *V* = 9528.0(7) Å³. Ni²⁺ cations are coordinated to four oxygen and two nitrogen atoms from four ligands and serve as 4-connected nodes. **X-dia-1-Ni-a1** is a 6-fold interpenetrated **dia** net (Figure 1c), interpenetration being enabled by adamantanoid cages with Ni...Ni edges of 17.2 Å. The accessible void volume available in **X-dia-1-Ni-a1** is 49 % despite the high level of interpenetration thanks to rectangular channels along the *c* axis (Figure 1d). The bulk purity of **X-dia-1-Ni-a1** was confirmed by PXRD experiments (Figure 1f).

Structural transformations of NiL₂. X-dia-1-Ni-a1 underwent single-crystal-to-single-crystal (SCSC) transformations after exchange with CH₂Cl₂ or heating at 85 °C for 24 h to less open phases, **X-dia-1-Ni-a2** and **X-dia-1-Ni-a3**, respectively (Figure S3). Whereas space group and connectivity are unchanged, reductions in cell volume (9528 to 8637 to 7441 Å³, for **a1-a3**, respectively), length of the *a* and *b* axis (24.20 to 22.17 to 19.95 Å for **a1-a3**, respectively) and solvent-accessible void volume (49, 43 and 33 % for **a1-a3**, respectively) accompanied the phase changes (Figure 1e and Figure S4). The adamantanoid cages exhibit Ni-Ni-Ni angles of 90°/120°, 80°/126° and 71°/132° for **a1-a3**, respectively. The breathing of the framework is accompanied by changes in N-Ni-N / C-Ni-C bond angles; 93.0°/101.5°, 90.7°/101.4° and 88.0°/102.4° for **a1-a3**, respectively (Table S3). **L** also undergoes conformational changes; the dihedral angle formed by the benzoate plane and the pyridine plane is perpendicular in **a1** (89.4°) but parallel in **a2**, (6.1°) and **a3** (1.8°). The breathing effect can be monitored by PXRD (Figure S5); lowest angle reflection (20) shifts from 2θ = 7.08° in **a1** to 2θ = 8.94° in **a3**.

Heating the **a1-a3** phases *in vacuo* results in a color change from dark green to light green and SCXRD revealed that the light green phase, **X-dia-1-Ni-c1**, is a non-porous **dia** net (orthorhombic space group *Pnn2*). Crystal morphology changes accompany the structural transformation (Figures 1f, 1g) as monitored by thermal microscopy. The Ni²⁺ cations of **X-dia-1-Ni-c1** adopt octahedral coordination geometry and serve as 4-connected nodes as in the open **a1-a3** forms. The planarity of **L** as quantified by the N(pyridyl)-phenyl-centroid-C(carboxylate) angle is 174° in **a1**, 176° in **a2**, 177° in **a3** and, remarkably, 155° in **c1** (Figure 1e). The Ni...Ni edges of the adamantanoid cages decrease from 17.2 Å (**a1**) to 16.3 Å (**c1**). We attribute the existence of **X-dia-1-Ni-c1** to the ability of **L** to contort and changes in the coordination geometry (Table S3). PLATON^[11] revealed that **X-dia-1-Ni-c1** has only 2% solvent-accessible volume. Overall, **X-dia-1-Ni-a1** undergoes a contraction of pore volume from 0.58 cm³g⁻¹ to 0.01 cm³g⁻¹ in **X-dia-1-Ni-c1** (Figure

1e). Such extreme structural transformations between closed and open phases are unusual. We are aware of only four previously reported FMOMs^[6b, 7c, 7d, 8d] that are known to exhibit such dramatic solvent or gas induced structural change (Table S4). The purity of the **c1** phase was confirmed by PXRD and synchrotron X-ray powder diffraction (SXRD) experiments. The SXRD pattern of **X-dia-1-Ni-c1** exhibits a diagnostic peak at 2θ = 5.58° (λ = 0.8269 Å) (Figure 1g). Thermogravimetric analysis of **X-dia-1-Ni-c1** indicated no weight loss until decomposition at 330 °C (Figure S6). **X-dia-1-Ni-c1** reverts to **X-dia-1-Ni-a1** when soaked in DMF or toluene at room temperature for 1 minute (Figure S7).

Multistep CO₂ adsorption isotherm. CO₂, with its large quadrupolar moment (13.4 × 10⁻⁴⁰ Cm²) and small kinetic diameter (3.3 Å), was chosen to probe how pressure affects switching between the open (**a1-a3**) and closed (**c1**) phases. The low-pressure adsorption isotherm of **X-dia-1-Ni** for CO₂ at 195 K exhibits multiple steps and the surface area of the least dense phase is 1641 m² g⁻¹ by Langmuir fitting (Figure 2a). There is strong hysteresis and clear steps are also present in the desorption isotherm. We conducted *in situ* PXRD and sorption coincident measurements^[12] (Figure 2b) by placing **X-dia-1-Ni-c1** on a copper plate under high vacuum before collecting PXRD data during CO₂ adsorption and desorption. The diagnostic low angle peak of the **c1** phase (10.03°, λ = 1.54178 Å) gradually diminished as the diagnostic peaks of **a3** (8.94°) and **a2** (7.93°) appeared, indicative of gate opening (Figure S8). The steep CO₂ uptake after 0.1 bar is consistent with transformation from **c1** to an open phase. The PXRD pattern did not change markedly in the pressure range 0.2–0.4 bar, which is consistent with the plateau observed in the adsorption isotherm. When CO₂ pressure was increased to 0.42 bar, the diagnostic low angle peak of **a1** (7.08°) appeared. The steep CO₂ uptake around 0.45 bar is consistent with a structural change from **a2** to **a1** that is complete at 0.77 bar. The *in situ* PXRD patterns on desorption indicate reversible structural changes between open and closed phases (Figure S9). **X-dia-1-Ni** exhibited no N₂ uptake at 1 bar and 77 K (Figure 2a).^[13] Simulations predict N₂ adsorption for **a1** (Figure 2a) and stepwise CO₂ adsorption at 195 K (Figure S17). The four steps in the 195 K CO₂ sorption isotherm of **X-dia-1-Ni** can be attributed to structural transformations as the framework switches from **c1** to **a3** to **a2** and, finally, to **a1**. That these transformations occur in SCSC fashion enables characterization of each phase in a manner that is atypical of FMOMs, which tend to be poorly crystalline following breathing or swelling.^[6b]

Methane storage performance of X-dia-1-Ni. Natural gas (NG), is mainly comprised of CH₄ and increasingly utilised for vehicular applications thanks to its geological abundance and low carbon footprint.^[14] Current storage technologies typically use cryogenic (liquefied NG at -161 °C, LNG) or high-pressure (compressed NG at 210–250 atm, CNG), conditions that are fraught with hazards and high costs. Adsorbed NG (ANG) using porous materials could mitigate these risks and costs. However, whereas 20,000+ physisorbent materials exist (e.g. activated carbons,^[15a] zeolites,^[15b] MOFs,^[15c, 15d] molecular crystals^[15e]), none yet offer volumetric working capacity that exceeds 200 v/v as offered by CNG (> 200 atm) at ambient temperature.

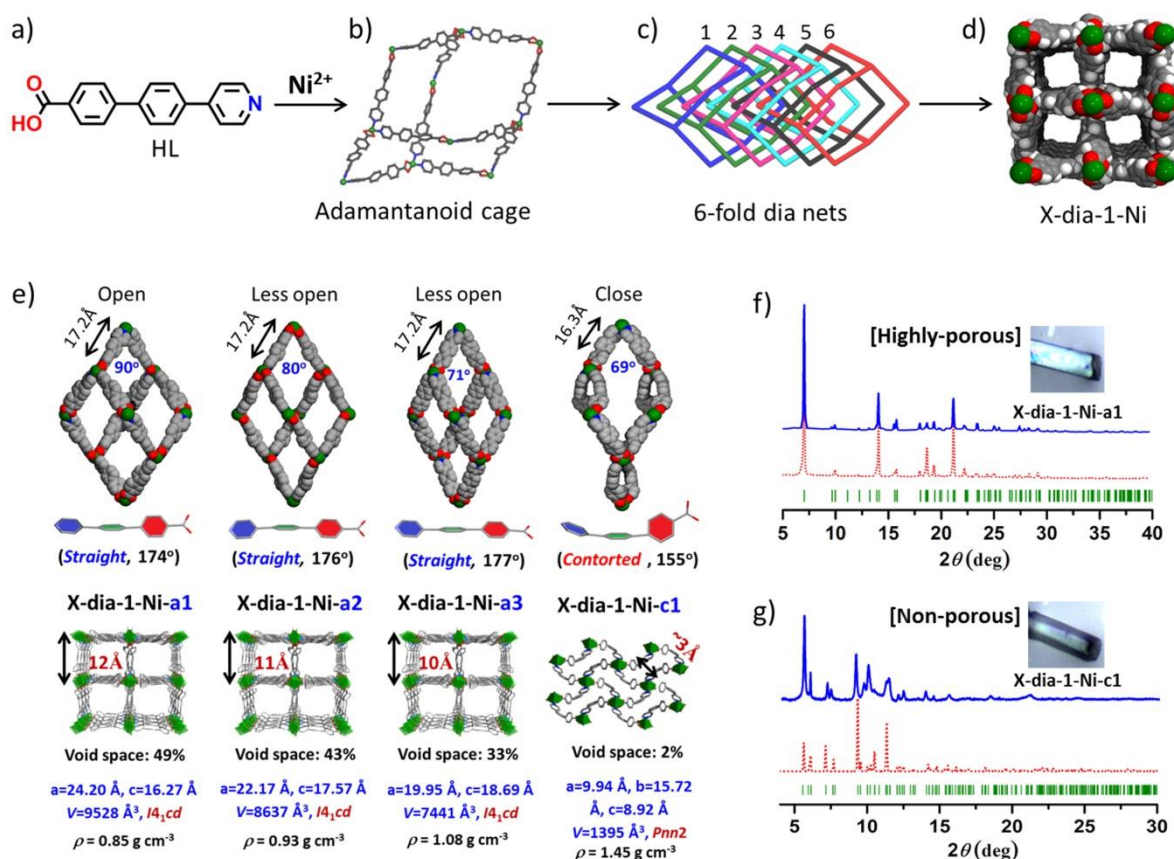


Figure 1. (a) Structure of 4-(4-pyridyl)-biphenyl-4-carboxylic acid (HL). (b) Adamantanoid cage in NiL₂. (c) 6-fold interpenetrated dia nets in NiL₂. (d) Rectangular channels viewed along the c-axis. (e) Single crystal structures of the porous (a1, a2, a3) and non-porous (c1) phases of X-dia-1-Ni. (f) Crystal morphology and PXRD pattern of a1. (g) Crystal morphology and synchrotron PXRD ($\lambda = 0.8262 \text{ \AA}$) pattern of c1.

A recent computational study of 650,000 porous materials^[16] suggests that no current class of rigid physisorbent is likely to exceed the working capacity of CNG. This is mainly because rigid materials typically exhibit type-I adsorption isotherms (Scheme 1a) and NG remains adsorbed at the typical deliverable pressure of 3-5 atm. Therefore, flexible materials that exhibit type F-IV isotherms as they switch between closed and open phases could achieve high working capacity that has eluded rigid sorbents (Scheme 1e). However, even before cost and stability issues are addressed, in order to be competitive with CNG, a flexible material must exhibit gate-opening above 5 atm and below storage pressure (e.g. 35 or 65 atm). In addition, storage capacity must be >200 v/v at 35 or 65 atm to compete with CNG. Unfortunately, most FMOMs transform between less open (narrow pore) and more open (large pore) phases (Scheme 1b, 1c). Indeed, we are aware of only 5 FMOMs^[7b, 7d, 8a-8c] that exhibit structure transformations between closed and open phases with appropriate NG gate opening pressure (5-35 atm), and only one exhibits high saturated uptake when open (Table S1).^[7d] NiL₂ is the second FMOM that meets these criteria. CH₄ adsorption isotherms measured at 298 K reveal that X-dia-1-Ni adsorbs minimal CH₄ below the phase change pressure (20 bar) and then exhibits an abrupt uptake in adsorption as switches to an open phase (Figure 3a). 285 K and 273 K CH₄ isotherms also exhibit a step but with increased

uptake before the step (Figure S21). *In situ* variable CH₄ pressure PXRD studies were conducted at 298 K by loading activated X-dia-1-Ni into a capillary and exposing the sample to methane (Figure S11). The kinetics of X-dia-1-Ni are too slow to observe phase changes the mixed metal variant (X-dia-1-Ni_{0.89}Co_{0.11}) more readily shows phase changes under pressure (Figure S12). X-dia-1-Ni_{0.89}Co_{0.11} is isomorphous to X-dia-1-Ni and was formed under the same conditions. Under vacuum, the c1 phase of X-dia-1-Ni_{0.89}Co_{0.11} is present whereas from 25 bar to 50 bar the peaks of the a1 phase appear. At 50 bar, X-dia-1-Ni_{0.89}Co_{0.11} had fully transformed to its a1 phase. The a1 phase fully converts to the c1 phase by around 5 bar. This phase change was also studied by P-DSC.^[17] An activated sample of X-dia-1-Ni was placed in a DSC sample chamber and exposed to CH₄ in the pressure range 1-50 bar at 298K. An exothermic peak at 25 bar is consistent with the phase change observed via *in situ* PXRD. The total CH₄ uptake of X-dia-1-Ni at 25 °C is 176 cm³ g⁻¹ (150 cm³ cm⁻³) for adsorption at 35 bar and 222 cm³ g⁻¹ (189 cm³ cm⁻³) at 65 bar. The potential working capacity, 147 cm³ cm⁻³ as calculated from adsorption isotherm between 35 bar and 5 bar, approaches that of benchmark MOFs (Table S5). However, hysteresis reduces the working capacity to 110 cm³ (5-35 bar) and 149 cm³ cm⁻³ (5-65 bar) respectively. Approaches to control hysteresis are being investigated.

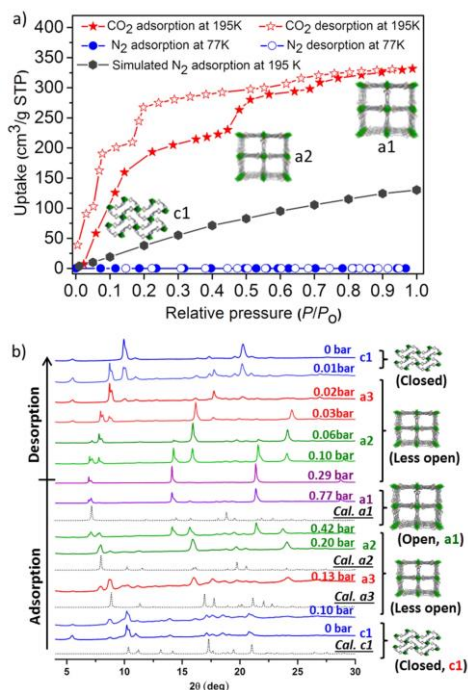


Figure 2. (a) Measured CO₂ (195K) and N₂ (77K) adsorption isotherms for **X-dia-1-Ni** and simulated N₂ (195 K) adsorption isotherm for **a1**. (b) *In situ* variable pressure PXRD ($\lambda = 1.54178 \text{ \AA}$) of **X-dia-1-Ni** at different CO₂ adsorption/desorption loadings collected at 195K. Calculated PXRD patterns are black. The PXRD patterns reveal that **X-dia-1-Ni** undergoes structural transformations from **c1** to **a3**, **a2** and then **a1**. Structural transformations from **a1** to **a2**, **a3** and **c1** occur during desorption.

Mechanism of structural flexibility. The mechanism of structural flexibility for FMOMs such as paddle-wheel based pillared-layered frameworks^[18] (the prototype for which is DMOF-1^[18a]), MIL-53,^[5a, 6a] and trigonal prism based networks such as MIL-88,^[6b] are based upon hinge motion associated with carboxylate coordination. Structural characterization of the various phases of **NiL₂** indicate a mechanism that largely relies upon ligand contortion. In addition, **c1** is stabilized by interactions between interpenetrated networks. We note that a similar **dia** network formed by a shorter linker ligand, 4-(4-pyridyl) benzoic acid, did not exhibit framework flexibility under the same conditions.^[10c] We attribute this to the lesser ability of shorter ligands to undergo extreme contortions of the type observed for **L**. Therefore, the key to the phase changes observed for this prototypal **X-dia** network is the use of the extended “X-ligand”, **L**. The single point energies of **L** in **a1** (Figure 4c) and **c1** (Figure 4a) were calculated at the MP2/aug-cc-pVDZ level of theory.^[19] The energy difference calculated between the two conformations of the ligand is +165 kJ mol⁻¹ (Figure 4b). Ligands that can contort during structural transformation are rare^[20] and no others are yet known to induce framework switching between closed and open phase. Ligand contortion and framework strain might be expected to lead to poor recyclability and reduced performance.^[8e] We indeed observed increases in pre-step adsorption at 298K after four sorption/desorption cycles (Figure S23b).

In summary, **X-dia-1-Ni** undergoes pressure and solvent induced SCSC transformations between closed and open phases. Four distinct phases of **X-dia-1-Ni** were isolated and studied by SC-XRD, PXRD and SXRD to provide structural insight into how ligand contortion can enable structural flexibility.

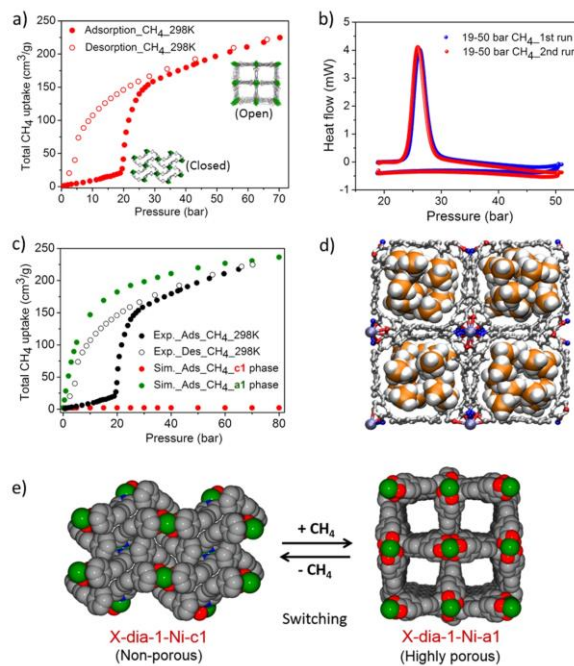


Figure 3. (a) Total CH₄ uptake isotherm at 298 K for **X-dia-1-Ni**. (b) Pressure-ramped DSC (CH₄, 298 K) for **X-dia-1-Ni**. (c) The simulated CH₄ adsorption isotherms in the open (**a1**) and closed (**c1**) phases of **X-dia-1-Ni** at 298 K with the experimental adsorption isotherm. (d) The modelled structure at CH₄ saturation in the open phase of **X-dia-1-Ni**. (e) Switching between closed (left) and open (right) phases of **X-dia-1-Ni** under CH₄ pressure.

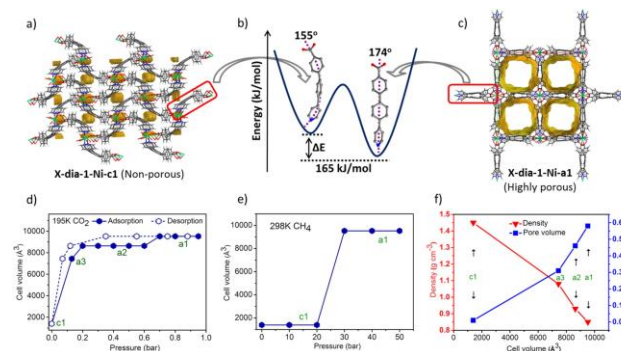


Figure 4. Crystal structures of the **c1** (a) and **a1** phases (c) of **X-dia-1-Ni**. (b) Conformation of **L** in the **c1** and **a1** phases. (d) Changes of cell volume of **X-dia-1-Ni** during CO₂ sorption. (e) Changes of cell volume of **X-dia-1-Ni** during CH₄ sorption. (f) Values of density and pore volume during transformation from **X-dia-1-Ni-c1** to **X-dia-1-Ni-a1**.

X-dia-1-Ni is only the second high surface area FMOM that exhibits CH₄ induced reversible switching with a type F-IV isotherm at pressures relevant for NG storage. Materials such as **X-dia-1-Ni** therefore have the potential to address storage and on-demand delivery of fuel gases by addressing both the working capacity and heat transfer issues that plague rigid sorbents. Perhaps most importantly, **X-dia-1-Ni** belongs to one of the longest studied and broadest classes of MOMs^[10a,21] and is therefore likely to be prototypal for a platform of related FMOMs that exhibit switching and type F-IV isotherms, but under different conditions. The possibility of fine-tuning of performance towards a particular gas under a particular set of conditions should be evident from this work.

Experimental Section

Crystallographic data for the structures reported in this paper have been deposited with the Cambridge Crystallographic Data Centre (CCDC 1426847-1426850).

Acknowledgements

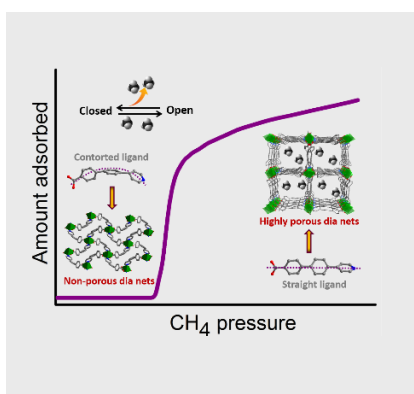
This work was generously supported by Science Foundation Ireland (SFI Award 13/RP/B2549). We thank K. Forrest for the simulations of adsorption isotherms. L.B. thanks the National Research Foundation of South Africa for financial support and PL thanks the Claude Leon Foundation for a postdoctoral fellowship. B.S. acknowledges the National Science Foundation (Award No. CHE-1152362), including support from the Major Research Instrumentation Program (Award No. CHE-1531590), the computational resources that were made available by a XSEDE Grant (No. TG-DMR090028), and the use of the services provided by Research Computing at the University of South Florida. N.H. and S. Kitagawa acknowledge the financial support of KAKENHI, Grant-in-Aid for Specially Promoted Research (No. 25000007) from the Japan Society of the Promotion of Science (JSPS). S. Kusaka and S. Kitagawa are thankful to the ACCEL program of Japan Science and Technology Agency (JST) for the financial support. We thank Diamond Light Source for access to beamline i11 (EE16167-1).

Keywords: flexible microporous materials • switching • stepped adsorption isotherm • contortion 4 • methane storage

- [1] C. A. Fyfe, G. J. Kennedy, C. T. De Schutter, G. T. Kokotailo, *J. Chem. Soc., Chem. Commun.* **1984**, 541-542.
- [2] a) S. Kitagawa, R. Kitaura, S.-i. Noro, *Angew. Chem. Int. Ed.* **2004**, *43*, 2334-2375; b) S. R. Batten, S. M. Neville, D. R. Turner, *Coordination Polymers: Design, Analysis and Application Introduction*, RSC Publishing, Cambridge, UK, **2009**.
- [3] a) T. R. Cook, Y.-R. Zheng, P. J. Stang, *Chem. Rev.* **2013**, *113*, 734-777; b) J. J. Perry IV, J. A. Perman, M. J. Zaworotko, *Chem. Soc. Rev.* **2009**, *38*, 1400-1417.
- [4] a) L. R. MacGillivray, *Metal-Organic Frameworks: Design and Application*, Wiley & Sons, **2010**; b) D. Farrusseng, *Metal-Organic Frameworks: Applications from Catalysis to Gas Storage*, Wiley-VCH, Weinheim, **2011**; c) H. Furukawa, K. E. Cordova, M. O'Keefe, O. M. Yaghi, *Science* **2013**, *341*, 1230444.
- [5] a) G. Férey, C. Serre, *Chem. Soc. Rev.* **2009**, *38*, 1380-1399; b) A. Schneemann, V. Bon, I. Schwedler, I. Senkowska, S. Kaskel, R. A. Fischer, *Chem. Soc. Rev.* **2014**, *43*, 6062-6096; c) S. Horike, S. Shimomura, S. Kitagawa, *Nat. Chem.* **2009**, *1*, 695-704; d) T. D. Bennett, A. K. Cheetham, A. H. Fuchs, F.-X. Coudert, *Nat. Chem.* **2016**, *9*, 11.
- [6] a) C. Serre, F. Millange, C. Thouvenot, M. Noguès, G. Marsolier, D. Louër, G. Férey, *J. Am. Chem. Soc.* **2002**, *124*, 13519-13526; b) C. Serre, C. Mellot-Draznieks, S. Surblé, N. Audebrand, Y. Filinchuk, G. Férey, *Science* **2007**, *315*, 1828-1831; c) A. Kondo, H. Noguchi, L. Carlucci, D. M. Proserpio, G. Ciani, H. Kajiro, T. Ohba, H. Kanoh, K. Kaneko, *J. Am. Chem. Soc.* **2007**, *129*, 12362-12363.
- [7] a) D. Li, K. Kaneko, *Chem. Phys. Lett.* **2001**, *335*, 50-56; b) R. Kitaura, K. Seki, G. Akiyama, S. Kitagawa, *Angew. Chem. Int. Ed.* **2003**, *42*, 428-431; c) V. Bon, N. Klein, I. Senkowska, A. Heerwig, J. Getzschmann, D. Wallacher, I. Zizak, M. Brzezinskaya, U. Mueller, S. Kaskel, *Phys. Chem. Chem. Phys.* **2015**, *17*, 17471-17479; d) J. A. Mason, J. Oktawiec, M. K. Taylor, M. R. Hudson, J. Rodriguez, J. E. Bachman, M. I. Gonzalez, A. Cervellino, A. Guagliardi, C. M. Brown, P. L. Llewellyn, N. Masciocchi, J. R. Long, *Nature* **2015**, *527*, 357-361.
- [8] a) H. Noguchi, A. Kondoh, Y. Hattori, H. Kanoh, H. Kajiro, K. Kaneko, *The Journal of Physical Chemistry B* **2005**, *109*, 13851-13853; b) K. Seki, *Phys. Chem. Chem. Phys.* **2002**, *4*, 1968-1971; c) P. L. Llewellyn, P. Horcajada, G. Maurin, T. Devic, N. Rosenbach, S. Bourrelly, C. Serre, D. Vincent, S. Loera-Serna, Y. Filinchuk, G. Férey, *J. Am. Chem. Soc.* **2009**, *131*, 13002-13008; d) Y.-S. Wei, K.-J. Chen, P.-Q. Liao, B.-Y. Zhu, R.-B. Lin, H.-L. Zhou, B.-Y. Wang, W. Xue, J.-P. Zhang, X.-M. Chen, *Chem. Sci.* **2013**, *4*, 1539-1546; e) N. Kavooosi, V. Bon, I. Senkowska, S. Krause, C. Atzori, F. Bonino, J. Pallmann, S. Paasch, E. Brunner, S. Kaskel, *Dalton Trans.* **2017**, *46*, 4685-4695.
- [9] a) J. Rabone, Y.-F. Yue, S. Y. Chong, K. C. Stylianou, J. Bacsá, D. Bradshaw, G. R. Darling, N. G. Berry, Y. Z. Khimyak, A. Y. Ganin, P. Wiper, J. B. Claridge, M. J. Rosseinsky, *Science* **2010**, *329*, 1053-1057; b) E. J. Carrington, C. A. McAnally, A. J. Fletcher, S. P. Thompson, M. Warren, L. Brammer, *Nat. Chem.* **2017**, *9*, 882-889; c) M. Shivanna, Q. Y. Yang, A. Bajpai, S. Sen, N. Hosono, S. Kusaka, T. Pham, K. A. Forrest, B. Space, S. Kitagawa, M. J. Zaworotko, *Sci. Adv.* **2018**, *4*, eaq1636; d) Y. Sakata, S. Furukawa, M. Kondo, K. Hirai, N. Horike, Y. Takashima, H. Uehara, N. Louvain, M. Meilikhov, T. Tsuruoka, S. Isoda, W. Kosaka, O. Sakata, S. Kitagawa, *Science* **2013**, *339*, 193-196.
- [10] a) M. J. Zaworotko, *Chem. Soc. Rev.* **1994**, *23*, 283-288; b) B. Moulton, M. J. Zaworotko, *Chem. Rev.* **2001**, *101*, 1629-1658; c) S. K. Elsaidi, M. H. Mohamed, L. Wojtas, A. Chanthapally, T. Pham, B. Space, J. J. Vittal, M. J. Zaworotko, *J. Am. Chem. Soc.* **2014**, *136*, 5072-5077.
- [11] A. L. Spek, *J. Appl. Crystallogr.* **2003**, *36*, 7-13.
- [12] H. Sato, W. Kosaka, R. Matsuda, A. Hori, Y. Hijikata, R. V. Belosludov, S. Sakaki, M. Takata, S. Kitagawa, *Science* **2014**, *343*, 167-170.
- [13] a) S. Yang, X. Lin, W. Lewis, M. Suyetin, E. Bichoutskaia, J. E. Parker, C. C. Tang, D. R. Allan, P. J. Rizkallah, P. Hubberstey, N. R. Champness, K. Mark Thomas, A. J. Blake, M. Schröder, *Nat. Mater.* **2012**, *11*, 710-716; b) Q.-Y. Yang, K.-J. Chen, A. Schoedel, L. Wojtas, J. J. Perry IV, M. J. Zaworotko, *CrystEngComm* **2016**, *18*, 8578-8581.
- [14] a) J. N. Armor, *J. Energy Chem.* **2013**, *22*, 21-26; b) D. Saha, H. A. Grappe, A. Chakraborty, G. Orkoulas, *Chem. Rev.* **2016**, *116*, 11436-11499.
- [15] a) D. Lozano-Castelló, J. Alcañiz-Monge, M. A. de la Casa-Lillo, D. Cazorla-Amorós, A. Linares-Solano, *Fuel* **2002**, *81*, 1777-1803; b) V. C. Menon, S. Komarneni, *J. Porous Mater.* **1998**, *5*, 43-58; c) Y. He, W. Zhou, G. Qian, B. Chen, *Chem. Soc. Rev.* **2014**, *43*, 5657-5678; d) Y. Peng, V. Krungleviciute, I. Eryazici, J. T. Hupp, O. K. Farha, T. Yildirim, *J. Am. Chem. Soc.* **2013**, *135*, 11887-11894; e) A. Pulido, L. Chen, T. Kaczorowski, D. Holden, M. A. Little, S. Y. Chong, B. J. Slater, D. P. McMahon, B. Bonillo, C. J. Stackhouse, A. Stephenson, C. M. Kane, R. Clowes, T. Hasell, A. I. Cooper, G. M. Day, *Nature* **2017**, *543*, 657.
- [16] C. M. Simon, J. Kim, D. A. Gomez-Gualdrón, J. S. Camp, Y. G. Chung, R. L. Martin, R. Mercado, M. W. Deem, D. Gunter, M. Haranczyk, D. S. Sholl, R. Q. Snurr, B. Smit, *Eng. Environ. Sci.* **2015**, *8*, 1190-1199.
- [17] P. M. Bhatt, E. Batisai, V. J. Smith, L. J. Barbour, *Chem. Commun.* **2016**, *52*, 11374-11377.
- [18] a) D. N. Dybtsev, H. Chun, K. Kim, *Angew. Chem. Int. Ed.* **2004**, *43*, 5033-5036; b) O. K. Farha, J. T. Hupp, *Acc. Chem. Res.* **2010**, *43*, 1166-1175; c) J. Seo, C. Bonneau, R. Matsuda, M. Takata, S. Kitagawa, *J. Am. Chem. Soc.* **2011**, *133*, 9005-9013.
- [19] H. Thom, Jr. Dunning, *J. Chem. Phys.* **1989**, *90*, 1007-1023.
- [20] a) P. Deria, D. A. Gómez-Gualdrón, W. Bury, H. T. Schaefer, T. C. Wang, P. K. Thallapally, A. A. Sarjeant, R. Q. Snurr, J. T. Hupp, O. K. Farha, *J. Am. Chem. Soc.* **2015**, *137*, 13183-13190; b) S. Krause, V. Bon, I. Senkowska, U. Stoeck, D. Wallacher, D. M. Többsen, S. Zander, R. S. Pillai, G. Maurin, F. O.-X. Coudert, S. Kaskel, *Nature* **2016**, *532*, 348-352.
- [21] B. F. Hoskins, R. Robson, *J. Am. Chem. Soc.* **1990**, *112*, 1546-1554.

COMMUNICATION

A new flexible coordination network, NiL_2 ($\text{L} = 4$ -(4-Pyridyl)-biphenyl-4-carboxylic acid), undergoes extreme structural transformations, enabled by ligand contortion, between non-porous (closed) and porous (open) phases as exemplified by stepped isotherm.



Qing-Yuan Yang, Prem Lama, Susan Sen, Matteo Lusi, Kai-Jie Chen, Wen-Yang Gao, Mohana Shivanna, Tony Pham, Nobuhiko Hosono, Shinpei Kusaka, John J. Perry IV, Shengqian Ma, Brian Space, Susumu Kitagawa, Leonard J. Barbour, and Michael J. Zaworotko*

Reversible switching between highly porous and non-porous phases of an interpenetrated diamondoid coordination network that exhibits gate-opening at methane storage pressures